Supplementary Information

Interface Engineering-Induced 1T-MoS_2/NiS Heterostructure for Efficient Hydrogen Evolution Reaction

Helei Wei [1,†], Aidong Tan [1,2,†], Wenbo Liu [1], Jinhua Piao [3], Kai Wan [1,*], Zhenxing Liang [1], Zhipeng Xiang [1,*] and Zhiyong Fu [1,*]

[1]Guangdong Provincial Key Laboratory of Fuel Cell Technology, School of Chemistry and Chemical Engineering, South China University of Technology, Guangzhou 510641, P.R. China

[2]Institute of Energy Power Innovation, North China Electric Power University, Beijing, 102206, P.R. China

[3]School of Food Science and Engineering, South China University of Technology, Guangzhou 510641, P.R. China

† These authors contributed equally to this work.

[*]Corresponding authors: E-mail: wank@scut.edu.cn (K. Wan), xzp20209094@scut.edu.cn (Z.P. Xiang), zyfu@scut.edu.cn (Z.Y. Fu)

Supplementary text

1. Chemicals

Nickel acetylacetonate ($Ni(acac)_2$, AR, Aladdin); nickel nitrate hexahydrate ($Ni(NO_3)_3 \cdot 6H_2O$, AR, Aladdin); molybdenum(VI) oxide (MoO_3, AR, 99.5%, Aladdin); potassium hydroxide (KOH, AR, 85%, Aladdin); 1-butylamine ($C_4H_{11}N$, AR, 99.99%, Aladdin); N, N-dimethylformamide (DMF, AR, 99.5 wt.%, Ghtech); potassium thiocyanate (KSCN, AR, 98.5 wt.%, Aladdin). All chemicals were used without any further purification.

2. Materials Preparation

2.1 Synthesis of 1T-MoS_2/NiS heterostructure

Synthesis of Ni nanosheet skeleton: The Ni nanosheet was synthesized as reported in the previous work.[1] Typically, 100 mg nickel acetylacetonate was dissolved in a mixture of 20.0 mL N, N-dimethylformamide, 1.0 mL 1-butylamine, and 4.0 mL deionized water. Then, transfer the above solution to a 50 mL para-polyphenyl (PPL) lined autoclave and react at 200 ^oC for 48 h. Finally, the gray-black powders were collected by centrifugation, washed with deionized water, and dried in a vacuum oven at 60 °C for 12 h to obtain the Ni nanosheet.

Synthesis of 1T-MoS_2/NiS heterostructure: 0.5 mmol Ni nanosheets as the framework, 1 mmol MoO_3, and 2.5 mmol KSCN were dissolved in a mixed solution of a certain proportion of ethanol and deionized water ($V_{ethanol}$: V_{water} = 1:4) under ultrasonic stirring for 60 min at room temperature to form a uniform solution. Then, transfer the above solution to a 50 mL polytetrafluoroethylene-lined reactor and react at 180 °C for 24 h. Finally, the gray-black powder was collected by centrifugation, washed with deionized water, and vacuum dried at 60 °C for 12 h to obtain the 1T-MoS_2/NiS heterostructure.

2.2 Synthesis of 2H-MoS_2 and 1T-MoS_2

The 2H-MoS_2 was synthesized using the same procedure as the 1T-MoS2/NiS heterostructure

without Ni nanosheets.

The 1T-MoS_2 was synthesized as reported in the previous work.[2] The process was as follows: 2H-MoS_2 was immersed in n-butyllithium solution at room temperature for 48 h. The nanostructures were exfoliated by reacting the intercalated lithium with excess water to produce H_2 gas and separated the 2D nanosheets, the resulting material was named 1T-MoS_2.

3. Physicochemical Characterization

The morphologies and microstructures were characterized by the scanning electron microscope (SEM, ZEISS Merlin, at 10 kV) and transmission electron microscope (TEM, JEM 2100, at 200 kV). The X-ray photoelectron spectroscopy (XPS) was carried out with a multi-technique system using an Al monochromatic X-ray at a power of 350 W (Thermo Scientific ESCALAB 250Xi). Atomic Force Microscope (AFM, Multimode 8, Bruker) was used to probe the thickness of materials. The X-ray diffraction (XRD) patterns were obtained using a Rigaku MiniFlex 600 X-ray diffractometer (Cu Kα radiation, λ = 1.54178 Å).

4. Electrochemical Measurements

The electrochemical hydrogen evolution reaction (HER) was performed in an Ar-saturated 1.0 M KOH solution at room temperature with a standard three-electrode system using a CHI730E electrochemical workstation. The working electrode was prepared as follows: 10 mg of powder is dispersed in 1.0 mL of Nafion/ethanol (0.84 wt.% Nafion) by ultrasonication for 30 min to obtain a homogeneous ink; then 50 μL of homogeneous ink was evenly drop-cast onto a carbon paper (1 × 1 cm^2, catalyst loading: 0.5 mg cm^{-2}). For comparison, the electrocatalytic activity of a commercial 40 wt.% Pt/C (HiSPEC4000, Johnson Matthey) for HER was evaluated at a metal loading of 20 μg cm^{-2}. The SCE was used as a reference electrode and Au mesh was used as the counter electrode.

The linear sweep voltammograms (LSVs) were recorded from -0.60 to 0.05 V *vs.* reversible

hydrogen electrode (RHE) with a scan rate of 5 mV s^{-1} in Ar-saturated 1.0 M KOH. The electrochemical impedance spectroscopy (EIS) was obtained in a frequency range from 100 kHz to 100 mHz with an amplitude of 5 mV at an applied potential of -0.05 V *vs.* RHE. Tafel slopes were derived from the LSV curves by fitting the data based on the Tafel equation: $\eta = a + b \cdot \log j$ (η is the overpotential, j is the current density, and b is the Tafel slope). The long-term stability testing was performed at a constant potential set at -0.12 V vs. RHE. All the electrochemical results were without *iR*-correction.

All the electrode potentials were calibrated to the RHE potential based on the Nernst equation $E_{RHE} = E_{Ref} + 0.0591\ V \times pH$ (E_{Ref} refers to the standard electrode potential of the reference electrode).

5. Computational Details

The DFT calculations were performed in the Quickstep code of the CP2K package based on the Gaussian and plane waves method (GPW). The Gaussian-type basis set was used to represent the Kohn-Sham orbitals and the plane-wave basis set was used to re-expand electron density in reciprocal space. The Gaussian basis set was molecularly optimized triple-zeta valence doubly polarized (TZV2P-MOLOPT) to describe the wave functions of H $1s^1$, O $2s^2 2p^4$, S $3s^2 3p^4$, Ni $3s^2 3p^6 3d^8 4s^2$, and Mo $4s^2 4p^6 4d^5 5s^1$ electrons, with a plane wave energy cut-off of 500 Ry, and norm-conserving Goedecker-Teter-Hutter (GTH) pseudopotentials were used to represent the rest core electrons of all elements. Perdew-Burke-Ernzerhof (PBE) functional was used to describe the nonlocal exchange and correlation energies. The Grimme D3 correction was applied in all calculations to correct the dispersion energy. The matrix diagonalization algorithm was selected to optimize the wave function and Fermi smearing with the electronic temperature of 300 K was selected to facilitate the self-consistent field (SCF) convergence.

During the calculation, the surface structure used is 1T-MoS_2 (002) with a 2-layer structure of a 3×3 supercell, and no atoms are fixed during the calculation. The supercell of 1T-MoS_2/NiS composed of a 1-layer MoS_2 unit and 3-layer NiS unit is selected, and all the atoms of the NiS layer are fixed in the calculation process.

Supplementary figures

The microscopic morphology of the Ni nanosheets framework was characterized by scanning electron microscope (SEM) and transmission electron microscope (TEM). As shown in Figure S1a-b, the resulting product shows a nanosheet morphology. The XRD pattern is consistent with the diffraction peak of the standard card Ni (PDF#87-0712), indicating the metallic Ni phase of the nanosheet (Figure S1c). The thickness of the prepared nickel nanosheets is confirmed by atomic force microscopy (AFM). As shown in Figure S1d-f, the thickness range is 1.65-4.64 nm, and the average thickness is about 3.2 nm.

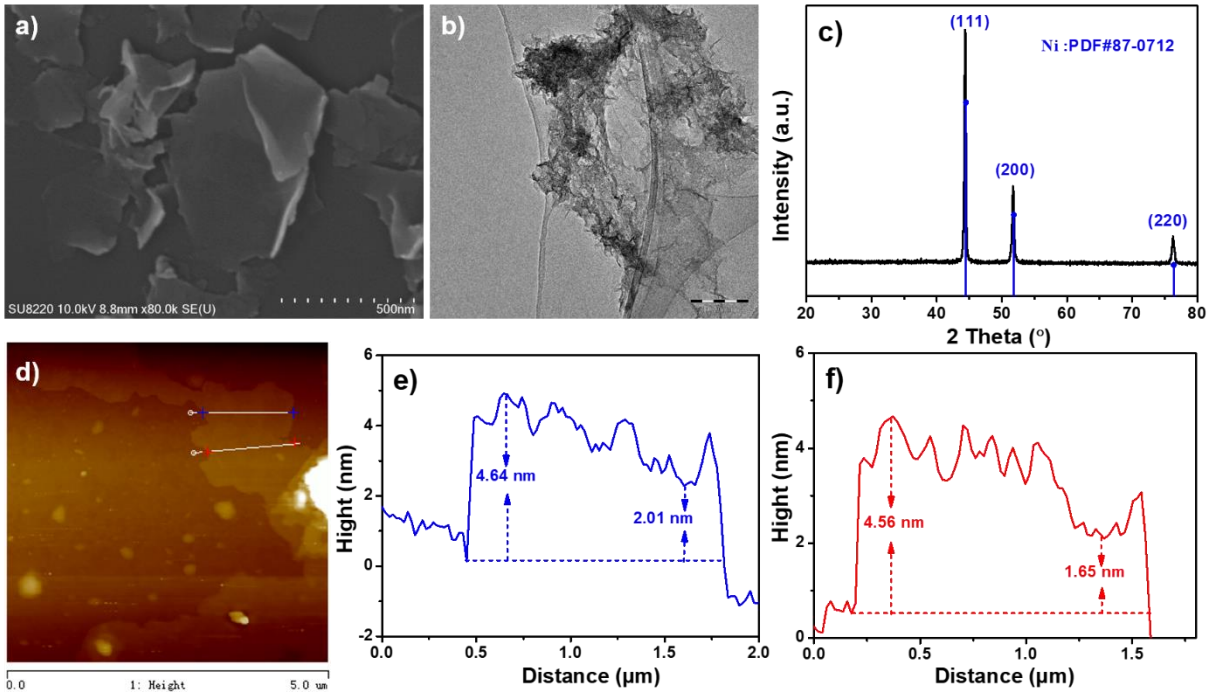

Figure S1. a) SEM image, b) TEM image and c) XRD pattern of the Ni nanosheets; d) AFM image and e-f) corresponding thicknesses.

As shown in Figure S2, only 2H-MoS_2 can be obtained without Ni nanosheets, which further confirms the induced phase transformation of interface engineering. The SEM and TEM images show that the resulting product of 2H-MoS_2 with a nanosheet morphology. The corresponding HRTEM image shows a lattice spacing of 0.62 nm, which correspond to the (002) crystal plane of 2H-MoS_2.[3] It is seen that the number of layers of 2H-MoS_2 nanosheets is distributed between 3-8 layers, which can provide numerous active sites. The crystal structure is shown in Figure S2d, which is consistent with the traditional 2H-MoS_2.[4]

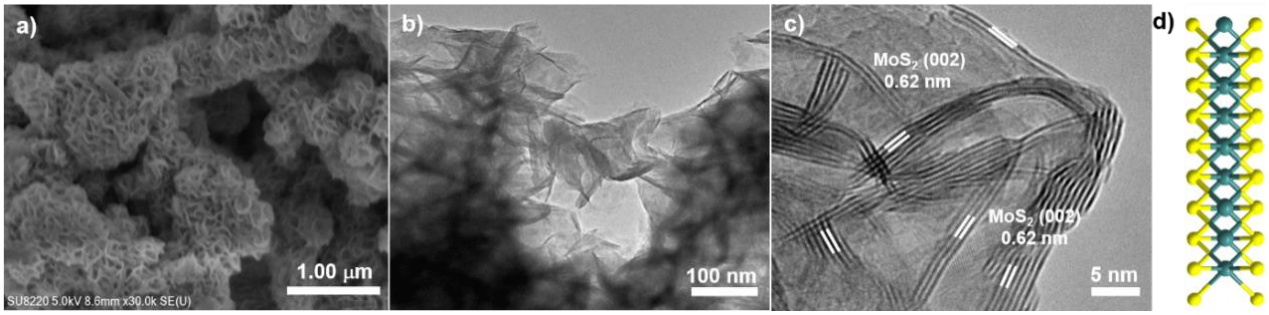

Figure S2. a) SEM image, b) TEM image and c) HRTEM image of the 2H-MoS_2; d) Crystal structure of 2H-MoS_2 nanosheets (S: yellow; Mo: dark green).

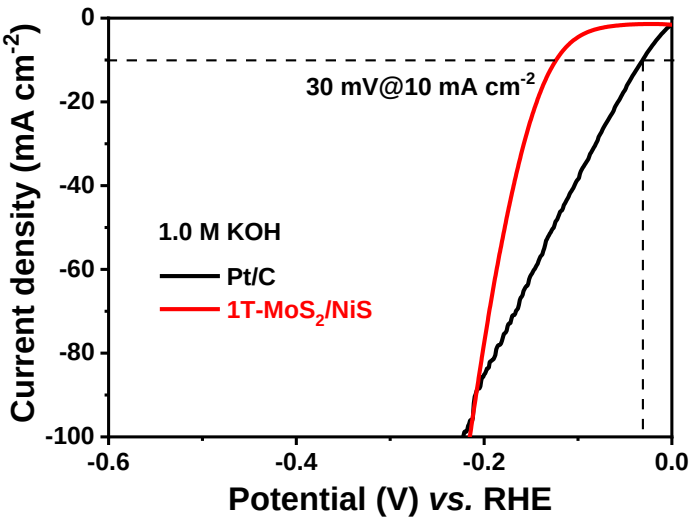

Figure S3. a) Polarization curves (without *iR* correction) of 1T-MoS_2/NiS and commercial Pt/C.

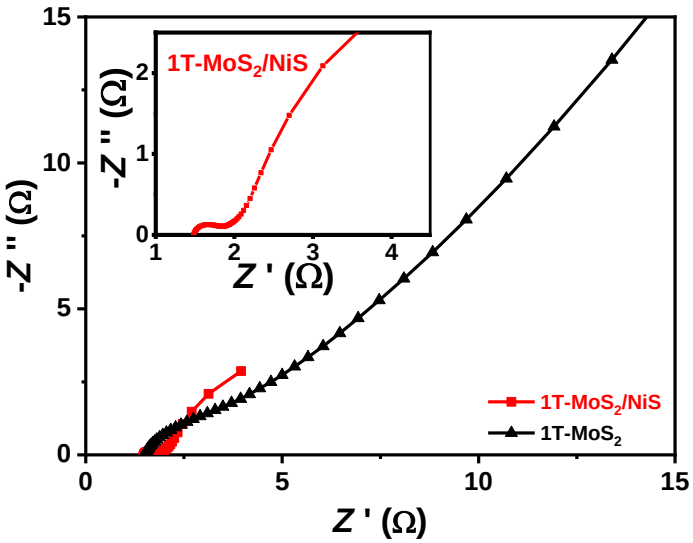

Figure S4. Nyquist plots of 1T-MoS_2/NiS and 1T-MoS_2 (inset is an enlarged view of 1T-MoS_2/NiS).

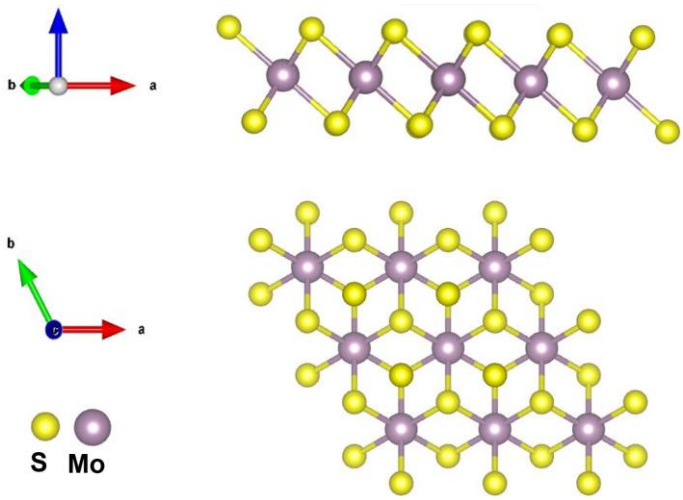

Figure S5. Side (above) and Top views (below) of the optimized slab models of 1T-MoS_2.

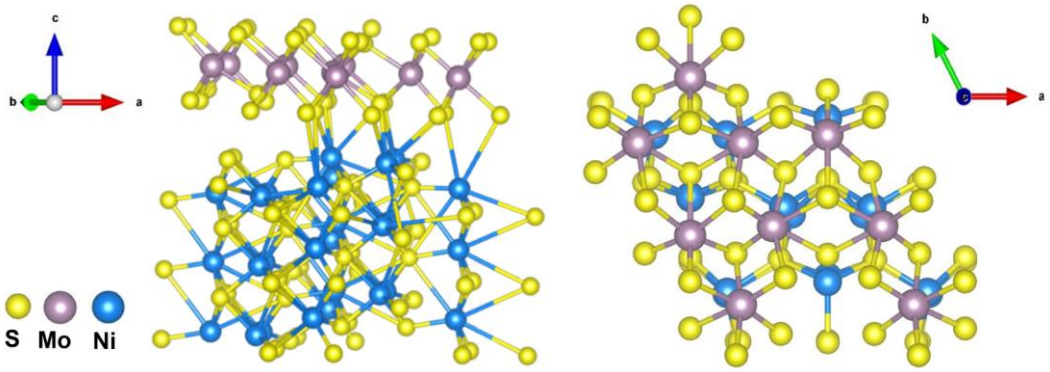

Figure S6. Side view (left) and top view (right) of the optimized plate model of the 1T-MoS_2/NiS.

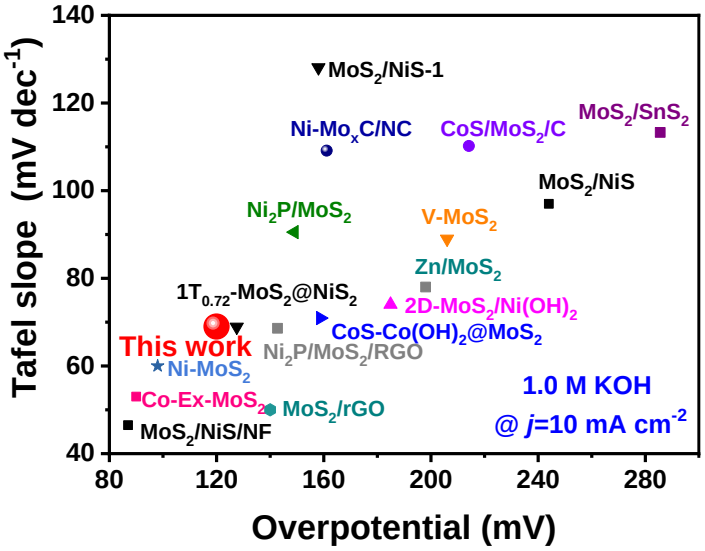

Figure S7. Performance comparison chart between different materials (data from Table S1, partly from Nat. Commun., 2021, 12, 5260).

Supplementary tables

Table S1. Comparisons of HER performance of the recently reported MoS_2-based electrocatalysts in 1.0 M KOH.

Catalysts	η@10 mA cm^{-2}	Tafel slope/dec^{-1}	Stability/h	Reference
1T-MoS_2/NiS	**120 mV**	**69**	**45**	**This work**
O-NiMoS	185 mV	80	10	(2018) ACS Catal. [5]
Zn-MoS_2	198 mV	78	6	(2019) Angew. Chem. Int. Ed. [6]
CoMoNiS-NF-31	113 mV	85	24	(2019) J. Am. Chem. Soc. [7]
MoS_2/NiS	244 mV	97	12	(2018) Small [8]
1T-MoS_2/NiS_2	116 mV	72	10	(2019) Angew. Chem. Int. Ed.[9]
S-MoS_2@C	155 mV	78	24	(2019) Adv. Energy Mater. [10]
MoS_2/NiS/NF	87 mV	47	40	(2020) Int. J. Hydrogen Energy [11]
MoS_2/NiS Core-Shell	84 mV	77	30	(2020) J. Power Sources. [12]
Ni-MoS_2	136 mV	72	20	(2020) Appl. Surf. Sci. [13]
Co_9S_8-MoS_2/NF	110 mV	82	60	(2020) Adv. Funct. Mater. [14]
Co-MoS_2	137 mV	59	--	(2021) Angew. Chem. Int. Ed.[15]
MoS_2/NLG-x	110 mV	106	140	(2021) ACS Catal. [16]
Ni-MoS_2/RGO	398 mV	140	--	(2021) Int. J. Electrochem. Sci. [17]
en-Bu-1T-MoS_2	169 mV	62	12	(2021) Chem. Eng. J. [18]
CoS_2@1T-MoS_2	72 mV	45	50	(2022) Appl. Catal. B: Environ [19]
MoS_2/NiS	158 mV	128	21	(2022) New J. Chem. [20]

References

1. Gao, S.; Lin, Y.; Jiao, X.; Sun, Y.; Luo, Q.; Zhang, W.; Li, D.; Yang, J.; Xie, Y., Partially Oxidized Atomic Cobalt Layers for Carbon Dioxide Electroreduction to Liquid Fuel. *Nature* **2016,** 529, 68-71.
2. Yin, Y.; Han, J.; Zhang, Y.; Zhang, X.; Xu, P.; Yuan, Q.; Samad, L.; Wang, X.; Wang, Y.; Zhang, Z.; Zhang, P.; Cao, X.; Song, B.; Jin, S., Contributions of Phase, Sulfur Vacancies, and Edges to the Hydrogen Evolution Reaction Catalytic Activity of Porous Molybdenum Disulfide Nanosheets. *J. Am. Chem. Soc.* **2016,** 138, 7965-7972.
3. Hu, J.; Zhang, C.; Jiang, L.; Lin, H.; An, Y.; Zhou, D.; Leung, M. K. H.; Yang, S., Nanohybridization of MoS_2 with Layered Double Hydroxides Efficiently Synergizes the Hydrogen Evolution in Alkaline Media. *Joule* **2017,** 1, 383-393.
4. Zang, Y.; Niu, S.; Wu, Y.; Zheng, X.; Cai, J.; Ye, J.; Xie, Y.; Liu, Y.; Zhou, J.; Zhu, J.; Liu, X.; Wang, G.; Qian, Y., Tuning Orbital Orientation Endows Molybdenum Disulfide with Exceptional Alkaline Hydrogen Evolution Capability. *Nat. Commun.* **2019,** 10, 1217.
5. Hou, J.; Zhang, B.; Li, Z.; Cao, S.; Sun, Y.; Wu, Y.; Gao, Z.; Sun, L., Vertically Aligned Oxygenated-CoS_2-MoS_2 Heteronanosheet Architecture from Polyoxometalate for Efficient and Stable Overall Water Splitting. *ACS Catal.* **2018,** 8, 4612-4621.
6. Wu, W.; Niu, C.; Wei, C.; Jia, Y.; Li, C.; Xu, Q., Activation of MoS_2 Basal Planes for Hydrogen Evolution by Zinc. *Angew. Chem. Int. Ed.* **2019,** 58, 2029-2033.
7. Yang, Y.; Yao, H.; Yu, Z.; Islam, S. M.; He, H.; Yuan, M.; Yue, Y.; Xu, K.; Hao, W.; Sun, G.; Li, H.; Ma, S.; Zapol, P.; Kanatzidis, M. G., Hierarchical Nanoassembly of $MoS_2/Co_9S_8/Ni_3S_2$/Ni as a Highly Efficient Electrocatalyst for Overall Water Splitting in a Wide pH Range. *J. Am. Chem. Soc.* **2019,** 141, 10417-10430.

8. Qin, Q.; Chen, L.; Wei, T.; Liu, X., MoS_2/NiS Yolk-Shell Microsphere-Based Electrodes for Overall Water Splitting and Asymmetric Supercapacitor. *Small* **2019,** 15, 1803639.

9. Chen, X.; Wang, Z.; Wei, Y.; Zhang, X.; Zhang, Q.; Gu, L.; Zhang, L.; Yang, N.; Yu, R., High Phase-Purity 1T-MoS_2 Ultrathin Nanosheets by Spatial Confined Template. *Angew. Chem. Int. Ed.* **2019,** 58, 17621-17624.

10. Xu, Q.; Liu, Y.; Jiang, H.; Hu, Y.; Liu, H.; Li, C., Unsaturated Sulfur Edge Engineering of Strongly Coupled MoS_2 Nanosheet-Carbon Macroporous Hybrid Catalyst for Enhanced Hydrogen Generation. *Adv. Energy Mater.* **2019,** 9, 1802553.

11. Xu, X.; Zhong, W.; Zhang, L.; Liu, G.; Du, Y., MoS_2/NiS Heterostructure Grown on Nickel Foam as Highly Efficient Bifunctional Electrocatalyst for Overall Water Splitting. *Int. J. Hydrogen Energy* **2020,** 45, 17329-17338.

12. Jiang, H.; Zhang, K.; Li, W.; Cui, Z.; He, S. A.; Zhao, S.; Li, J.; He, G.; Shearing, P. R.; Brett, D. J. L., MoS_2/NiS Core-Shell Structures for Improved Electrocatalytic Process of Hydrogen Evolution. *J. Power Sources* **2020,** 472, 228497.

13. Gaur, A. P. S.; Zhang, B.; Lui, Y. H.; Tang, X.; Hu, S., Morphologically Tailored Nano-Structured MoS_2 Catalysts via Introduction of Ni and Co Ions for Enhanced HER Activity. *Appl. Surf. Sci.* **2020,** 516, 146094.

14. Kim, M.; Anjum, M. A. R.; Choi, M.; Jeong, H. Y.; Choi, S. H.; Park, N.; Lee, J. S., Covalent 0D-2D Heterostructuring of Co_9S_8-MoS_2 for Enhanced Hydrogen Evolution in All pH Electrolytes. *Adv. Funct. Mater.* **2020,** 30, 2002536.

15. Duan, H.; Wang, C.; Li, G.; Tan, H.; Hu, W.; Cai, L.; Liu, W.; Li, N.; Ji, Q.; Wang, Y.; Lu, Y.; Yan, W.; Hu, F.; Zhang, W.; Sun, Z.; Qi, Z.; Song, L.; Wei, S., Single-Atom-Layer Catalysis in a MoS_2 Monolayer Activated by Long-Range Ferromagnetism for the Hydrogen Evolution

Reaction: Beyond Single-Atom Catalysis. *Angew. Chem. Int. Ed.* **2021,** 60, 7251-7258.

16. Qin, J.; Xi, C.; Zhang, R.; Liu, T.; Zou, P.; Wu, D.; Guo, Q.; Mao, J.; Xin, H.; Yang, J., Activating Edge-Mo of 2H-MoS_2 via Coordination with Pyridinic N-C for pH-Universal Hydrogen Evolution Electrocatalysis. *ACS Catal.* **2021,** 11, 4486-4497.

17. Zhao, M., One Step Hydrothermal Synthesis of Ni-MoS_2-RGO Bifunctional Electrocatalysts for HER and OER. *Int. J. Electrochem. Sci.* **2021,** 16, 210323.

18. Vedhanarayanan, B.; Shi, J.; Lin, J. Y.; Yun, S.; Lin, T. W., Enhanced Activity and Stability of MoS_2 through Enriching 1T-Phase by Covalent Functionalization for Energy Conversion Applications. *Chem. Eng. J.* **2021,** 403, 126318.

19. Liu, Z.; Wang, K.; Li, Y.; Yuan, S.; Huang, G.; Li, X.; Li, N., Activation Engineering on Metallic 1T-MoS_2 by Constructing In-Plane Heterostructure for Efficient Hydrogen Generation. *Appl. Catal. B: Environ.* **2022,** 300, 120696.

20. Zhao, X.; Bao, J.; Zhou, Y.; Zhang, Y.; Sheng, X.; Wu, B.; Wang, Y.; Zuo, C.; Bu, X., Heterostructural MoS_2/NiS Nanoflowers Via Precise Interface Modification for Enhancing Electrocatalytic Hydrogen Evolution. *New J. Chem.* **2022,** 46, 5505-5514.